Inorganic Chemistry

Article

pubs.acs.org/IC

Structural Study of Hydrated/Dehydrated Manganese Thiophene-2,5-diphosphonate Metal Organic Frameworks, $Mn_2(O_3P-C_4H_2S-PO_3)\cdot 2H_2O$

Jean-Michel Rueff,*[,†] Olivier Perez,[†] Alain Pautrat,[†] Nicolas Barrier,[†] Gary B. Hix,[‡] Sylvie Hernot,[§] Hélène Couthon-Gourvès,[§] and Paul-Alain Jaffrès*[,§]

[†]CRISMAT, UMR CNRS 6508, ENSICAEN, Université de Caen Basse-Normandie, 6 Boulevard du Maréchal Juin, 14050 Caen, France

[‡]School of Science and Technology, Nottingham Trent University, Nottingham NG11 8NS, United Kingdom

[§]Université de Brest and Université Européenne de Bretagne, CNRS UMR 6521, CEMCA, IFR 148 ScInBios, 6 Avenue Victor Le Gorgeu, 29238 Brest, France

Supporting Information

ABSTRACT: Synthesis of thiophene-2,5-diphosphonic acid **2** is reported, and its use for synthesis of the original pristine materials $Mn_2(O_3P-C_4H_2S-PO_3)\cdot 2H_2O$ **3** is reported. The structure of material **3** has been fully resolved from single-crystal X-ray diffraction. $Mn_2(O_3P-C_4H_2S-PO_3)\cdot 2H_2O$ **3** crystallizes in a monoclinic cell (space group *P*2) with the following parameters: a = 11.60(1) Å, b = 4.943(5) Å, c = 19.614(13) Å, β = 107.22°. A noticeable feature of the structure of compound **3** is the orientation of the thiophene heterocycles that adopt two different orientations in two successive layers (along c). Thermal analysis of compound **3** indicates that the water molecules are easily removed from 160 to 230 °C while the dehydrated structure is stable up to 500 °C. The dehydrated compound obtained from **3** can be rehydrated to give the polymorphic compound $Mn_2(O_3P-C_4H_2S-PO_3)\cdot 2H_2O$ **4**, which crystallizes in an orthorhombic cell (space group *Pnam*) with the following parameters: a = 7.5359(3) Å, b = 7.5524(3) Å, c = 18.3050(9) Å. The main difference between the structures of **3** and **4** arises from both the orientation of the thiophene rings (herringbone-type organization in **4**) and the structure of the inorganic layers. The thiophene-2,5-diphosphonic acid moieties engaged in materials **3** and **4** adopt a different orientation likely due to rotation around the P−C bonds and via the dehydrated state **5**, which is likely more flexible than the hydrated states. Study of the magnetic properties performed on compound **3** and **4** and on the dehydrated compounds $Mn_2(O_3P-C_4H_2S-PO_3)$ **5** complemented by the structural study has permitted us to characterize the antiferromagnetic ground state of sample **3**, a weak ferromagnetic component in sample **4**, and complete paramagnetic behavior in sample **5**.

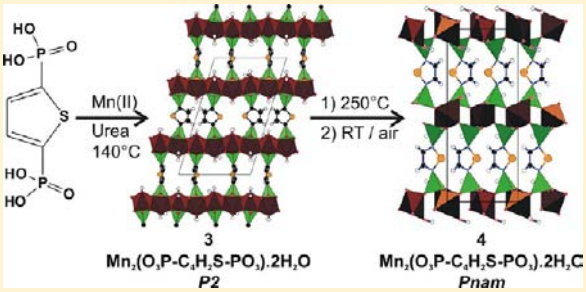

INTRODUCTION

Over the last decades, metal organic frameworks (MOF) have been extensively studied with the aim of identifying new families of molecular materials that could be used for new applications.[1] A key question regards the rules that, at an atomic scale, govern the assembly of the primary building units (organic and inorganic building blocks) to form successively the secondary building units (SBU) and the final materials.[2] Rigid,[3] flexible,[4] or semiflexible[5] organic building blocks have been engaged in the synthesis of MOF with the aim of evaluating the consequences of their intrinsic flexibility on the topology of the resulting materials. It noticeable that the use of rigid polyfunctional organic precursors has produced a wide variety of hybrid materials that have been studied for their properties in diverse fields including magnetism,[6] luminescence,[7] catalysis,[8] gas storage,[9] or drug release.[10] For the design of such materials, the carboxylic acid functional group has played a central role since many carboxylate and polycarboxylate derivatives are commercially available and others were specifically designed.[11]

Besides the use of carboxylic acid derivatives to design MOF, other functional groups including phosphonic acids[12] or sulfonic acids[13] have been used to produce original structures that exhibit interesting properties. In particular, the presence of two different functional groups (heteropolyfunctional organic precursors) has proved to be a valuable strategy to produce materials with singular properties. Indeed, Morris et al. synthesized a material with two carboxylic acid and one sulfonic acid functional groups linked to a rigid motif (e.g., a benzene ring). This material exhibits at the solid state a reversible bond breaking that involves connection of organic molecules with the inorganic network.[14] Synthesis of phosphonic acid, polyphosphonic,[15] or phosphonic−carboxylic

Received: June 5, 2012
Published: September 20, 2012

   dx.doi.org/10.1021/ic301187y | *Inorg. Chem.* 2012, 51, 10251−10261

derivatives has also produced materials exhibiting interesting properties (e.g., microporosity[16]). We previously synthesized and used rigid polyfunctional organic precursors in which a benzene ring acts as a rigid platform.[17] According to this strategy the use of 4-carboxyphenylphosphonic acid **A** (Scheme 1) when reacted with an europium salt produced a luminescent

Scheme 1. Chemical Structure of Compounds A–C and 2

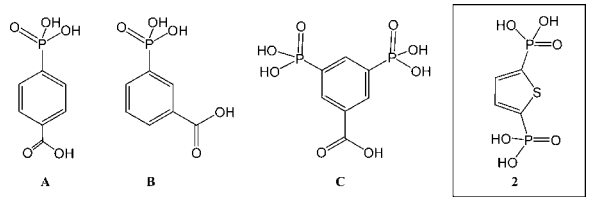

material characterized by its high thermal stability.[18] Reaction of the carboxylic–phosphonic derivative **B** with copper salts gives rise to a homochiral helical structure.[19] The same organic precursor **B** reacted with zinc nitrate has produced a 2D or 3D hybrid material depending on the pH of the reaction media, illustrating the possibility with some experimental conditions to observe chemoselectivity in the course of hybrid material construction.[20] Finally, compound **C** when combined with a copper salt produced a complex 3D structure[21]made of inorganic columns connected by organic parts.

On the basis of these results, which clearly indicate the relevance of studying further the use of rigid phosphonic or polyphosphonic derivatives for construction of hybrid materials, functionalization of thiophene has come to our attention. Indeed, in the literature, several materials based on the use of thiophene–carboxylate or thiophene–dicarboxylate as organic building blocks are reported; these materials are interesting for both their structures and their properties. Indeed, thiophene-2,5-dicarboxylate (TDC) gives rise to several kinds of connections between the carboxylate function and the inorganic network,[22] and diverse properties (luminescence,[23] chiral material,[24] magnetism[25,29]) have been reported.

To the best of our knowledge, use of the phosphonic acid equivalent of thiophen–carboxylate for design of hybrid structure has been only seldom investigated. One study reports the use of thiophene-2-phosphonic or thiophene-3-phosphonic acids for construction of a hybrid structure following an organometallic route of synthesis that makes use of dimethylzinc ($ZnMe_2$) as the inorganic source.[26] In that study, the layered structure of the zinc–phosphonate hybrid material was confirmed by powder X-ray diffraction and the structure was further investigated by solid state NMR. A second study reports the use of thiophene-2-phosphonic acid for modification of TiO_2 surfaces.[27] In that instance, the organic compound acts as an interface modifier for design of photovoltaic devices. We aim to report herein the first use of thiophene-2,5-diphosphonic acid **2** (Scheme 1) for construction of hybrid materials. Materials produced were obtained as single crystals, allowing unambiguous description of the structure. Complementary characterization, including the thermal stability and magnetic properties of these compounds, is reported.

EXPERIMENTAL SECTION

General. All compounds were fully characterized by ^1H, ^{13}C, and ^{31}P NMR spectroscopy (Bruker AC 300 spectrometer). The following abbreviations were used: s singlet, d doublet, t triplet, m multiplet. Elemental analyses were recorded with an automatic apparatus CHNS-O Thermo-Quest. Infrared (IR) spectroscopy spectra were recorded on a FTIR Thermo Nicolet FT-IR Nexus spectrometer working in absorbance mode in the 400–4000 cm^{-1} range at 4 cm^{-1} optical resolution. A powder sample was diluted by mixing KBr (2 wt %). Mass spectroscopy analyses were performed on a Bruker Autoflex MALDI TOF-TOF III LRF200 CID. Thermogravimetric analyses (TGA) were recorded at a rate of 3 °C/min from 30 to 800 °C under air or nitrogen gas flow using a SETARAM TGA 92 apparatus. Differential scanning calorimetry (DSC) was performed at a rate of 10 °C/min from 10 to 280 °C under nitrogen gas flow using a Perkin Elmer DSC 4000 apparatus equipped with an Intracooler.

The magnetic susceptibility and magnetic moment of the different samples were measured in a SQUID MPMS (Quantum design). Magnetic suceptibilities were recorded as a function of temperature using a zero-field-cooling procedure or a field-cooling–zero-field-cooling procedure (B = 0.1 T).

Scanning electron microscopy (SEM) and energy-dispersive spectroscopy (EDS) have been performed using a Zeiss Supra 55 electron microscope.

Tetraethyl Thiophene-2,5-diphosphonate 1. $NiBr_2$ (0.48 g ; 2.2 mmol), 2,5-dibromothiophene (3.6 g, 14.8 mmol), and mesitylene (10 mL) were placed under a nitrogen atmosphere in a two-neck round-bottom flask fitted with a reflux condenser and an addition funnel. The suspension was heated at 180 °C, and triethylphosphite (7.4 g, 44.5 mmol) was carefully added dropwise for 30 min. At the end of the addition, the solution was heated further at 180 °C for 6 h. After cooling to room temperature, the volatiles, including the solvent, were removed in vacuo. Dichloromethane (50 mL) was added, and the solution was washed with water (3 × 50 mL). The organic phase was dried over $MgSO_4$, filtered, and concentrated in vacuo to produce an oil. After purification by column chromatography on silica gel (CH_2Cl_2/MeOH: v/v 100/2) compound **1** was isolated in 85% yield (4.5 g) as a pale yellow oil.

^1H NMR (300.13 MHz, $CDCl_3$): 1.34 (m, O–CH_2-CH_3), 4.17 (m, O–CH_2-CH_3), 7.63 (d, $^3J_{HH}$ = 5.5 Hz, C*H*), 7.65 (d, $^3J_{HH}$ = 5.6 Hz, C*H*). ^{31}P NMR (121.49 MHz, $CDCl_3$): 9.98 (s). ^{13}C NMR (75.47 MHz, $CDCl_3$): 16.1 (s, O–CH_2-CH_3), 62.9 (s, O-CH_2–CH_3), 136.1 (dd, $^1J_{CP}$ = 203.7 Hz, $^3J_{CP}$ = 5.7 Hz, *C*-P), 136.2 (d, $^2J_{CP}$ = 15.2 Hz, C=C–P), 136.4 (d, $^2J_{CP}$ = 15.3 Hz, C=C–P). MS (MALDI-TOF): m/z calcd for $C_{12}H_{23}O_6P_2S$ (M + H) 357.069; found 357.057.

Thiophene-2,5-diphosphonic Acid 2. A 9 mL (67.3 mmol) amount of trimethylsilylbromide was added to a solution of tetraethyl thiophene-2,5-diphosphonate **1** (4 g, 11.2 mmol) in dry methylene chloride (80 mL). The mixture was stirred at room temperature for 12 h and concentrated in vaccuo. The residue was recovered in 150 mL of methanol and stirred at room temperature for 1 h. Following evaporation of methanol, diphosphonic acid **2** was quantitatively obtained (2.7 g) as a white crystalline solid (See Supporting Information, Figure SI1, for X-ray powder diffraction).

^1H NMR (300.13 MHz, D_2O): 4.33 (s large, OH), 7.36 (d, $^3J_{HH}$ = 5.5 Hz, C*H*), 7.37 (d, $^3J_{HH}$ = 5.6 Hz, C*H*). ^{31}P NMR (121.49 MHz, D_2O): 7.25 (s). ^{13}C NMR (75.47 MHz, $CDCl_3$): 135.1 (d, $^2J_{CP}$ = 15.5 Hz, C=C–P), 135.3 (d, $^2J_{CP}$ = 15.5 Hz, C=C–P), 137.7 (dd, $^1J_{CP}$ = 203.0 Hz, $^3J_{CP}$ = 6.3 Hz, *C*-P). Anal. Calcd for $C_4H_6O_6P_2S$ (244.10): C, 19.68; H, 2.48; S, 13.14. Found: C, 19.10; H, 2.40; S, 12.72.

Hydrothermal Synthesis of $Mn_2(O_3P–C_4H_2S–PO_3)·2H_2O$ 3. Thiophene-2,5-diphosphonic acid **2** (0.05 g, 0.2 mmol), urea (0.024 g, 0.4 mmol), and $Mn(NO_3)_2·6H_2O$ (0.118 g, 0.4 mmol) were dissolved in distilled water (15 mL). The resulting solution was placed in a PTFE insert of 50 mL. After stirring 15 min the pH of the mother solution ($pH_{initial}$) was 1.66. The insert was then transferred in a Berghof pressure digestion vessel and heated from room temperature to 140 °C in 20 h, heated 40 h at 140 °C, and cooled to room temperature in 40 h. At the opening of the PTFE insert the pH of the solution (pH_{final}) was 4.13, and the final material, obtained as light brown crystals with suitable size for structure resolution on a single crystal, was isolated by filtration, washed with water rinsed with absolute ethanol, and dried in air.

dx.doi.org/10.1021/ic301187y | *Inorg. Chem.* 2012, 51, 10251–10261

A pattern matching of the whole preparation realized from the single-crystal data permitted us to confirm that compound **3** was obtained as a single phase (see Supporting Information, Figure SI2, for pattern matching from single-crystal data).

$Mn_2(O_3P-C_4H_2S-PO_3)\cdot 2H_2O$ (**3**): yield 0.06 g (78%). Anal. Calcd: C, 12.45; H, 1.57. Found: C, 12.57; H, 1.86. IR (KBr): 3517, 3457.7, 3107.8, 1604.9, 1504.8, 1428.2, 1299.7, 1287.9, 1222.9, 1207.3, 1099.9, 1070.6, 1043.7, 1003.3, 972.8, 841.6, 816.4, 755.9, 749.3, 611.6, 591.7.

RESULTS AND DISCUSSION

Synthesis and Characterization of the Materials. Thiophene-2,5-diphosphonic acid **2** was synthesized in a two-step sequence that makes use of 2,5-dibromothiophene as a starting material (Scheme 2). In a first step substitution of the

Scheme 2. Synthesis of Thiophene-2,5-diphosphonic Acid, 2[a]

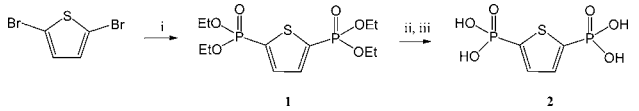

[a](i) $NiBr_2$, triethylphosphite, mesitylene, 180 °C. (ii) Me_3SiBr, CH_2Cl_2. (iii) MeOH.

two bromide atoms using a nickel-assisted Arbuzov reaction (Tavs's method[28]) produced tetraethyl thiophene-2,5-diphosphonate **1** in 85% yield. In this reaction the use of nickel bromine, $NiBr_2$, which gives rise to more reproducible results, is preferred compared to $NiCl_2$, which is generally used for synthesis of arylphosphonates from arylbromides. Direct hydrolysis of the diphosphonate **1** with concentrated HCl proved to be unsuccessful. Indeed, the expected product was contaminated by side products attributed to breaking of one P−C bond as confirmed by ^{31}P NMR, which indicated the presence of phosphate at 0.3 ppm (D_2O). Therefore, use of milder conditions, previously used for synthesis of thiophene-2-phosphonic acid by Gerbier et al.,[26] were tested. Hydrolysis of the phosphonate function was achieved in a two-step sequence that starts by silylation of the diphosphonate **1** with bromotrimethylsilane. Then the silylated intermediate was quantitatively converted into the expected diphosphonic acid **2** by reaction with methanol. With this mild method of hydrolysis, the thiophene−diphosphonic acid **2** was isolated without any trace of the degradation product as revealed by NMR data and elemental analysis.

Compound **2** was used in hydrothermal syntheses along with manganese salt ($Mn(NO_3)_2.6H_2O$), water, and urea (see Experimental Section). The pH of the initial solution, measured 15 min after stirring the substrates in water, was 1.66, and the final pH (measured at the opening of the pressure vessel) was 4.13. From this reproducible hydrothermal synthesis (140 °C, 40 h) single crystals from the compound $Mn_2(O_3P-C_4H_2S-PO_3)\cdot 2H_2O$ **3** with suitable size that allowed characterization by X-ray diffraction were produced. Pictures recorded by scanning electron microscopy (SEM) permitted us to confirm the homogeneity of platelet shape of the crystals in the synthesis batch and their average size of 200 × 200 × 4 μm (Figure 1).

The infrared spectrum of $Mn_2(O_3P-C_4H_2S-PO_3)\cdot 2H_2O$ **3** is shown in Figure SI3 (see Supporting Information). The infrared spectra have at low wavenumbers, between 700 and 1300 cm^{-1}, the typical bands of the phosphonate functional group. At higher wavenumbers, spectra exhibit at 1608 cm^{-1}

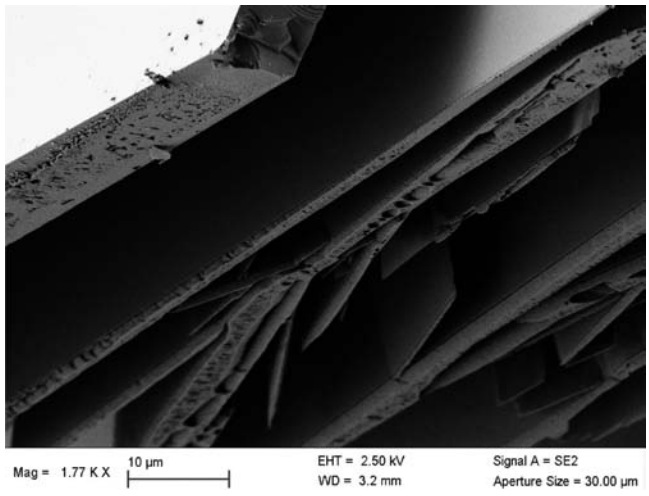

Figure 1. Representative crystal of $Mn_2(O_3P-C_4H_2S-PO_3)\cdot 2H_2O$ **3** with a platelet shape observed by SEM.

the characteristic band of the water bending vibration (δ H_2O). Spectra reveal also in the 3000 cm^{-1} wavenumber region the symmetric (υ_s H_2O) and at higher wavenumber the asymmetric (υ_{as} H_2O) stretching bands of lattice water molecules: 3461 and 3528 cm^{-1}. Finally, the stretching vibration band of the aromatic C−H bond[29] is observed at 3108 cm^{-1}.

Thermogravimetric curves recorded in air (Figure 2) exhibit a first mass loss between 150 and 250 °C, which is ascribed to

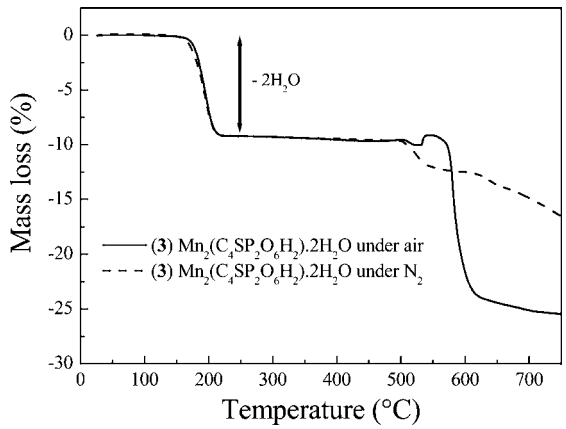

Figure 2. TGA curves of $Mn_2(O_3P-C_4H_2S-PO_3)\cdot 2H_2O$ **3** recorded in air or N_2 from room temperature to 750 °C.

loss of two molecules of coordination water present around the transition metal: 9.12% for $Mn_2(O_3P-C_4H_2S-PO_3)\cdot 2H_2O$ (theoretical loss 9.3%). After 500 °C, a second mass loss is observed and attributed to transformation of the dehydrated materials into the corresponding transition metal phosphate clearly identified by powder X-ray diffraction and for which formation is in good agreement with the total mass loss recorded: $Mn_2P_2O_7$ for $Mn_2(O_3P-C_4H_2S-PO_3)\cdot 2H_2O$ (obs 25.4%; calcd 26.4%). Mass gain observed just before final decomposition of the material has been attributed to an oxidation process, which was confirmed by thermogravimetric analysis performed under nitrogen to not exhibit such mass gain. It is interesting to observe that the temperature of degradation of the dehydrated structure that likely occurs according to a combustion reaction is observed above 450 °C, which is a slightly higher temperature than that observed for the

dx.doi.org/10.1021/ic301187y | Inorg. Chem. 2012, 51, 10251−10261

compound {Co(thiophene-2,5-dicarboxylate)$(H_2O)_{1.5}]_n$.[29] The presence of a phosphorus atom is one parameter that can explain this gain of thermal stability.

Data Collection and Structure Determination. Crystals with regular platelet shapes and shining faces were extracted from batch synthesis. The preliminary X-ray diffraction investigation was performed at room temperature using Mo Kα radiation on a Kappa CCD (Bruker Nonius) diffractometer. Large ω and χ scans were used to control the crystalline quality of the different samples and determine cell parameters. All tested specimens lead to the following cell: a_1 = 4.9684(4) Å, b_1 = 5.8105(6) Å, c_1 = 18.793(3) Å, $\alpha_1 = \beta_1 = \gamma_1 \approx 90°$. A first data collection was performed using a middle-sized single crystal (150 × 80 × 5 μm^3). A scanning angle of 0.8°/frame and a D_x (detector−sample distance) value of 34 mm have been chosen; ϕ and ω scans were used. The observed condition limiting the possible reflections, *hkl*: $h + k + l = 2n$, is consistent with an *I* centering vector, and the following space groups can be considered: *Immm*, *Im2m*, *I2mm*, *Imm2*, $I2_12_12_1$, and *I*222. EvalCCD software[30] was used to extract reflections from the collected frames. Empirical absorption correction was applied using the SADABS software.[31] Symmetry determination following structure solution in *P*1 was performed using the "charge flipping" method[32] implemented in SUPERFLIP;[33,34] it leads to space group *I*2*mm*. A structural model considering the *I*2*mm* space group was then built up with SUPERFLIP[33] using the charge flipping method. Manganese, phosphorus, sulfur, oxygen, and 2 carbon atoms were located; at this stage the carbons, not implied in the coordination sphere of the phosphorus, are missing. This first model is introduced in the refinement program Jana2006;[35] all atomic positions were refined, and then anisotropic displacement parameters (ADP) are considered for all atoms. Fourier difference synthesis does not allow location of the final expected carbon atoms. Moreover, a huge value is observed along the *b* axis for ADP of the sulfur atom S ($u_{22} \approx 0.39$ Å^2), 10 times those observed along the *a* or *c* axis. Final refinement based on the *F*(obs) procedure leads to *R*(obs) = 0.095 and *wR*(obs) = 0.131. The absence of two carbons in this structural analysis could be related to a disorder due to possible rotation of the thiophene cycle around the axis defined by the two phosphorus−carbon bonds.

To confirm previous results, data collection was performed using the same experimental conditions but a larger crystal (300 × 150 × 6 μm^3). The (0*kl*) section of reciprocal space calculated from the series of experimental frames shows rows of weak additional reflections located at $k = n/2$; this (0*kl*) plane is indicated in Figure 3. On the basis of this observation, a new cell can be defined to index the whole diffraction pattern: a_2 = 11.621(1) Å, b_2 = 4.9684(4) Å, c_2 = 19.670(3) Å, β_2 = 107.181(3)°. The relationship with the previous cell is as follows

$$a_2 = 2b_1;\ b_2 = -a_1;\ c_2 = -b_1 + c_1$$

To collect a great number of weak reflections, but avoiding any detector saturation by reflections of strong intensity, two different exposure times (160 and 32 s/deg) have been used to collect data. Diffracted intensities were collected up to θ = 40°. No condition limiting possible reflections is observed, and then the possible space groups are *P*2/*m*, *Pm*, and *P*2. EvalCCD software[30] was used to extract reflections from the collected frames; reflections were merged and rescaled as a function of the exposure time. Empirical absorption correction was applied using the SADABS software.[31] Details of data collection are reported in Table 1.

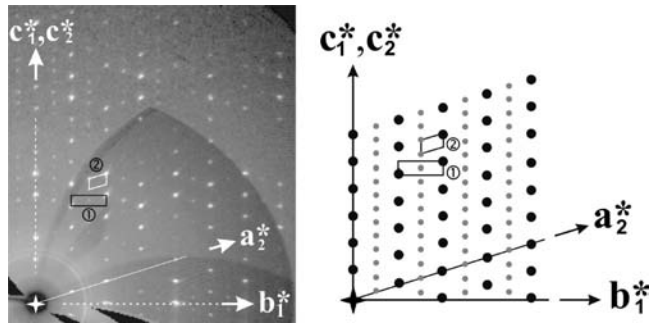

Figure 3. $Mn_2(O_3P{-}C_4H_2S{-}PO_3){\cdot}2H_2O$ **3** section of the reciprocal space ((0*kl*) for the (a_1, b_1, c_1) setting) calculated from the experimental frames (left) and the corresponding drawing (right). Cells ① and ② are reported. Intense reflections allowing definition of cell ① are depicted using black disks, while weak reflections are represented using gray dots.

Table 1. Details of Data Collection for Compounds 3 and 4[a]

	hydrated **3**	rehydrated **4**
chemical formula	$Mn_2(O_3P{-}C_4H_2S{-}PO_3){\cdot}2H_2O$	$Mn_2(O_3P{-}C_4H_2S{-}PO_3){\cdot}2H_2O$
symmetry	monoclinic	orthorhombic
lattice centring	primitive	primitive
a, Å	11.60(1)	7.5359(3)
b, Å	4.943 (5)	7.5524(3)
c, Å	19.614 (13)	18.3050(9)
β (deg)	107.22 (6)	90
space group	*P*2	*Pnam*
wavelength (Å)	0.71073	0.71073
scan strategy	φ /ω	φ /ω
scan angle (deg)/D_x (mm)	0.8/34	0.8/34
$(\sin\theta/\lambda)_{max}$	0.86	0.94
reflns index limit	$-20 \le h \le 13$	$-14 \le h \le 12$
	$-5 \le k \le 8$	$-14 \le l \le 8$
	$-35 \le l \le 35$	$-34 \le k \le 34$
measd reflns	16 622	22 606
unique reflns	8028	3701
unique refls with $I \ge 3\sigma(I)$	3213	2560
abs corr	SADABS[31]	SADABS[31]
internal *R* value after correction (obs/all)	0.026/0.037	0.031/0.041
refinement program	JANA200635	JANA200635
number of refinement parameters	226	119
weighting method	σ	σ
ρ_{min}/ρ_{max} (e/Å^3)	2.43/−4.56	−0.6/0.5
F(000)	618	760
reliability factors (*R*/*Rw*)	0.039/0.039	0.043/0.071
goodness of fit	1.60/1.55	1.45/1.34

[a]Reliability factors are based on *F*.

Following the procedure described above a structure solution was performed in *P*1 space group using SUPERFLIP.[33,34] The electron density corresponding to the final model is compatible with the *P*2 space group; structure determination carried out in the *P*2/*m* or *Pm* space group does not lead to satisfactory solution. The structural model in this space group, including 4 Mn, 4 P, and 2 S atoms, is then introduced in the refinement

dx.doi.org/10.1021/ic301187y | *Inorg. Chem.* 2012, 51, 10251−10261

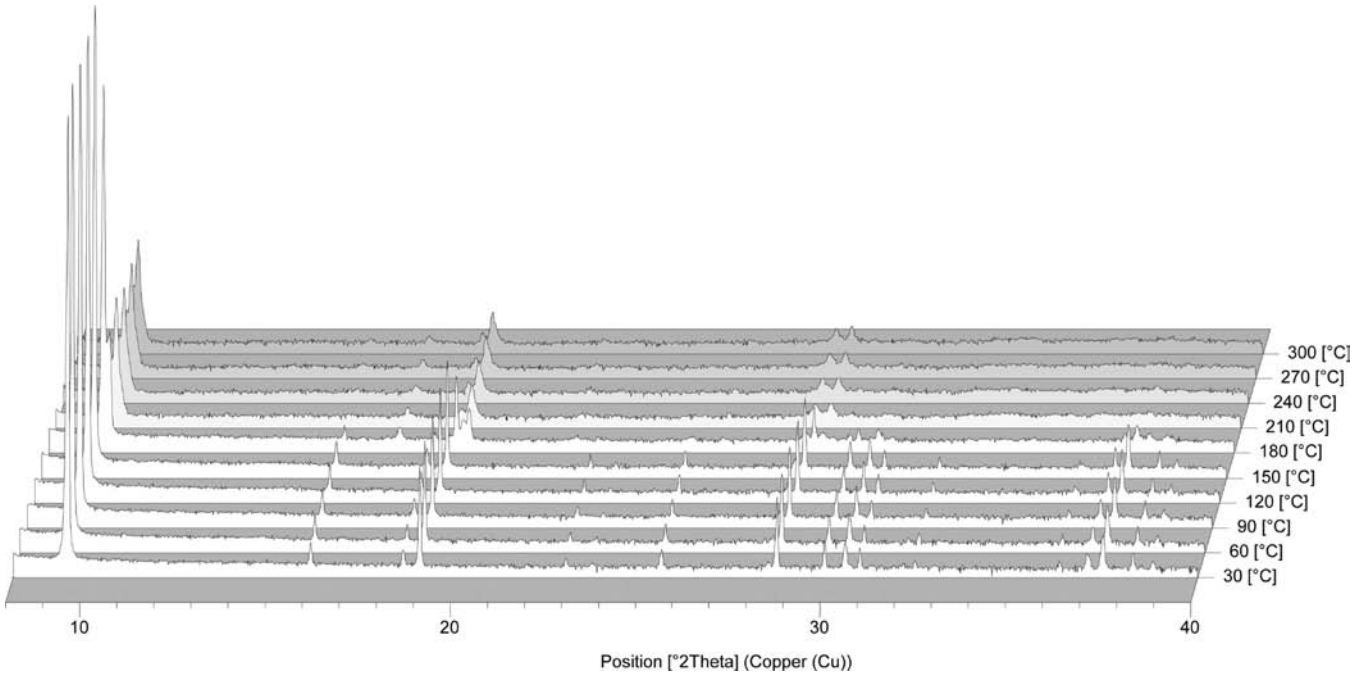

Figure 4. Diffraction patterns collected of $Mn_2(O_3P{-}C_4H_2S{-}PO_3){\cdot}2H_2O$ **3** versus temperature.

program Jana2006;[35] all atomic positions were refined, and then ADP are considered for all atoms. Refinement leads to an agreement factor equal to 14%. Fourier differences were then calculated, allowing the location of 16 oxygen and 8 carbon atoms. Then, applying a (sin θ/λ) limit equal to 0.5, regions where the contribution of the H atoms to the structure factors is larger, Fourier difference synthesis is used to find the H atoms. Eight H atoms are found in the coordination sphere of O atoms; the bond valence calculations[36] for the oxygen atoms are in agreement with introduction of these H atoms. Two independent $Mn_2(O_3P{-}C_4H_2S{-}PO_3){\cdot}2H_2O$ motifs are observed. The final refinement procedure leads to R(obs) = 0.039 and wR(obs) = 0.039. The value refined for the Flack parameter[37] (0.510(3)) is compatible with a twinned crystal. Atomic parameters are summarized in Tables SI1 and SI2 (see Supporting Information), and interatomic distances are listed in Table SI3, Supporting Information. Note that use of the very weak additional reflections greatly contributes to the high noise level observed on the Fourier difference maps; these data essential for determining the thiophene cycles are of lower quality.

As previously discussed, the thermogravimetric analyses (TGA) show the stabilization of a dehydrated phase above 250 °C, the temperature where the pristine compound loses 2 water molecules, and below 500 °C, final decomposition. A selection of crystals of the pristine material **3** were weighed and heated above 250 °C. The experiment was stopped when the expected loss of weight, corresponding to 2 H_2O, was obtained; the resulting sample (compound **5**) will be called "dehydrated". To analyze the structure of this dehydrated compound, a single-crystal X-ray diffraction experiment was placed with the "heated" crystals. However, a breakdown of the detector of our KappaCCD diffractometer has delayed this study. After 1 month and fixing the detector problem, single crystals of the heated sample have been tested using X-ray diffraction. All tested crystals show the same characteristics. The following cell parameters are evidenced: a_3 = 7.5359(3) Å, b_3 = 7.5524(3) Å, c_3 = 18.3050(9) Å, $\alpha_3 = \beta_3 = \gamma_3 = 90°$. A strategy based on ϕ and ω scans (scan angle of 0.8°/frame with an exposure time of 96s/frame; an extra scan with an exposure time of 9 s/frame has been considered to avoid the saturation effect expected for intense reflections) was defined for θ_{max} = 42° and D_x = 34 mm. The values observed for the internal reliability factor for the *mmm*, 4/*mmm*, and 4/*m* Laue class (0.085, 0.583, and 0.563, respectively) are in favor of orthorhombic symmetry.

Structure determination was performed using SUPERFLIP;[33] a starting point has been obtained but with misnamed oxygen and carbon atoms. The model including corrections of the atoms designation has been introduced in JANA2006;[35] the structure can be described with 1 Mn, 1 P, 1S, 4O, and 2 C atoms. All atomic positions and ADP were refined. The reliability factor reaches a value of 0.063. Fourier difference synthesis shows important residues around the Mn position (2.3 e·Å^{-3}). Introduction for Mn and S of anharmonic ADP developed up to the fourth order leads to a significant reduction of the agreement factor (R_{Fobs} = 0.049). Fourier difference synthesis calculated for sin $\theta/\lambda \leq 0.5$ evidences residues compatible with 1 H atom in the neighborhood of 1 C and 2 H in the vicinity of 1 O atom. Introduction of these two H atoms in the environment of this oxygen reveals an improvement of bond valence calculation[36] (0.48 without the two H and 1.9 with). The final stage of the refinement leads to the same chemical formula, $Mn_2(O_3P{-}C_4H_2S{-}PO_3){\cdot}2H_2O$, as for the pristine compound **3**; it is incompatible with a dehydrated compound. TGA performed on the remaining part of the "dehydrated" sample evidences a rehydration process in agreement with the refinement result. Actually, the studied structure does not correspond to a dehydrated but to a rehydrated form identified as compound **4**. Atomic parameters are summarized in Tables SI4 and SI5 (see Supporting Information), and a selection of distances and angles are listed in Table SI6, Supporting Information.

X-ray Powder Diffraction versus Temperature. To follow the structural evolution of the compound $Mn_2(O_3P{-}C_4H_2S{-}$

dx.doi.org/10.1021/ic301187y | *Inorg. Chem.* 2012, 51, 10251−10261

$PO_3)\cdot 2H_2O$ **3** as a function of temperature, X-ray powder diffraction patterns were collected on a Bruker D8 diffractometer in Bragg−Brentano geometry using Cu $K\alpha_1$ radiation (1.54056 Å), selected by an incident germanium monochromator, and equipped with a Lynx-Eye detector and an Anton Paar HTK1200N high-temperature chamber. Diagrams were collected using a step scan of ~0.014°/2θ ranging from 6° to 60°/2θ, recorded every 30 °C between 30 and 300 °C, and summarized in Figure 4. This study shows that the monoclinic structure corresponding to the hydrated form is stable until 150 °C and in the range of temperature corresponding to the dehydratation process (see TGA analysis part Figure 2). Refinements of the unit cell parameters versus temperature reveal that the *c* axis corresponding to the stacking direction is constant until 90 °C and then decreased until 150 °C and confirms that loss of H_2O starts above 90 °C. At 180 °C the X-ray diffraction diagrams correspond to a mixture of the monoclinic hydrated related phase and the new dehydrated phase **5**. The X-ray diffraction diagrams at higher temperatures show broad diffraction peaks, which are consistent with a poor crystalline quality of the dehydrated phase. Nevertheless, this latter material **5** could be indexed in an orthorhombic unit cell with the following parameters: a = 18.632 Å; b = 18.354 Å; c = 5.064 Å at 210 °C. In parallel, several "freshly dehydrated" crystals of compound **5** were tested on the KappaCCD; the scattering signal is mainly diffuse and thus confirms the amorphization process observed by powder diffraction.

Structural Description. *Hydrated $Mn_2(O_3P-C_4H_2S-PO_3)\cdot 2H_2O$* ***3***. The hydrated form $Mn_2(O_3P-C_4H_2S-PO_3)\cdot 2H_2O$ **3** can be described by the regular stacking along the *c* axis of $[MnO_6H_2]_\infty$ inorganic planes and organic slabs built up from $(O_3P-C_4H_2S-PO_3)$ entities (see Figure 5 and Scheme 3). In the $[MnO_6H_2]_\infty$ inorganic planes, displayed in the Figure 6b, each Mn atom is surrounded by 6 oxygen atoms, assuming six Mn−O distances ranging from 2.09 to 2.44 Å (Table SI3, Supporting Information). The 6 O atoms define a distorted octahedron around the Mn atoms. Each MnO_6 octahedron shares 5 corners with 5 adjacent octahedra and one edge with a PO_3C tetrahedron of one $(O_3P-C_4H_2S-PO_3)$ entity (see Figure 6a); the last corner is occupied by a water molecule. Inside the inorganic plane, the shortest Mn−Mn distances ranged from 3.81 to 3.91 Å (Table SI3, Supporting Information). Two consecutive $[MnO_6H_2]_\infty$ inorganic planes are connected to the other via the two phosphonic acid functional groups present on the thiophenyl heterocycle in positions 2 and 5; this conformation leads to interplane Mn−Mn distances ranging from 8.8 to 9.9 Å (Table SI3, Supporting Information). A description of the $(O_3P-C_4H_2S-PO_3)$ organic planes can be based on the observations of Figure 5a and 5b. The conformation of the thiophene heterocycles (C_4H_2S) is different for levels 1 and 2 identified in Figure 5. In level 1, the cycles are oriented parallel to the *b* axis, while in level 2 they are parallel to the *a* axis. This arrangement of the (C_4H_2S) cycles is reported in Figure 7a, where cycles belonging to two successive levels are drawn for a projection along [001].

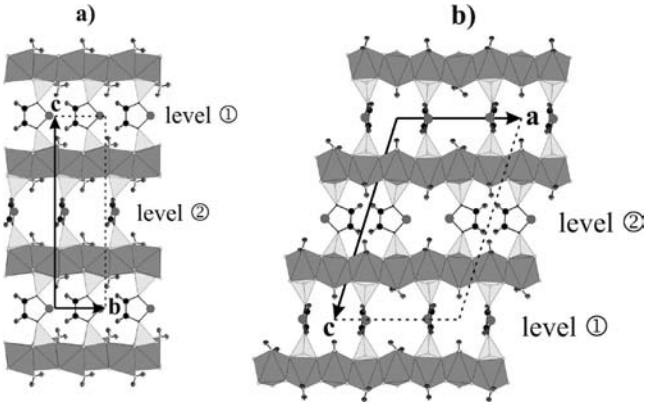

Figure 5. $Mn_2(O_3P-C_4H_2S-PO_3)\cdot 2H_2O$ **3** projection along the *a* (a) and *b* axes (b). MnO_6 and PO_3C are represented by gray and light gray polyhedra. S, C, and H atoms are represented by gray, black, and crossed disks, respectively.

Scheme 3. Coordination Modes of the Phosphonic Acid Functions of the Thiophene-2,5-diphosphonic Acid Moiety (TDP) Included in $Mn_2(O_3P-C_4H_2S-PO_3)\cdot 2H_2O$ 3

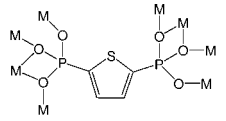

$(\kappa^2\text{-}\kappa^2\text{-}\kappa^1\text{-}\mu_4)\text{-}(\kappa^2, \kappa^2, \kappa^1\text{-}\mu_4)\text{-}\mu_8 TDP^{4-}$

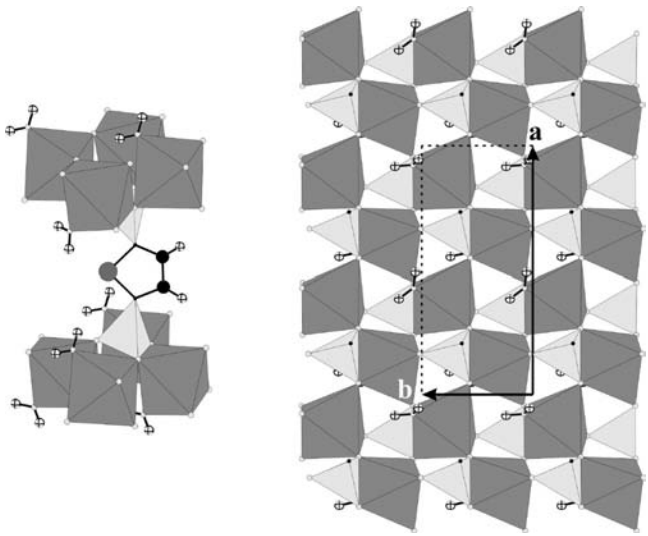

Figure 6. $Mn_2(O_3P-C_4H_2S-PO_3)\cdot 2H_2O$ **3** (a) view of the connexion between the inorganic layers and the $(O_3P-C_4H_2S-PO_3)$ unit, and (b) projection along the *c* axis of one inorganic layer (including phosphonate groups).

Rehydrated $Mn_2(O_3P-C_4H_2S-PO_3)\cdot 2H_2O$ ***4***. The rehydrated $Mn_2(O_3P-C_4H_2S-PO_3)\cdot 2H_2O$ **4** adopts a layered structure; stacking in the direction *b*, $[Mn_2O_8H_4]_{dimer}$ inorganic planes alternate regularly with slabs of $(O_3P-C_4H_2S-PO_3)$ entities constituting the organic part of the material (see Figure 8). In the $[Mn_2O_8H_4]_{dimer}$ inorganic planes, displayed in Figure 9c, each Mn atom is surrounded by 5 oxygen atoms; the four closer oxygen neighbors (with 1.97 Å $\leq d_{Mn-O} \leq$ 2.00 Å) form a pseudosquare plane; the fifth O atom assumes a longer Mn−O distance (d_{Mn-O} = 2.41 Å) (see Table SI6, Supporting Information). Thus, the 5 O atoms define a slightly distorted square pyramid around the Mn atoms. Two adjacent square pyramids share an edge; they are arranged in a head-to-tail way and form a $Mn_2O_8H_4$ unit shown in Figure 9b. The two O2 edges of these edifices are water molecules; the six remaining O edges are connected to six P1 atoms (Figure 9c). As a result, each $Mn_2O_8H_4$ unit is isolated from the other unit; this feature

dx.doi.org/10.1021/ic301187y | *Inorg. Chem.* 2012, 51, 10251−10261

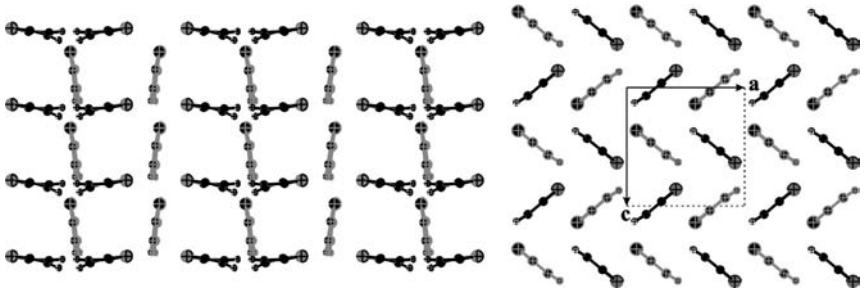

Figure 7. Projections along [001] of the hydrated form **3** (a) and along the *b* axis for the rehydrated form **4** (b). Only the C_4H_2S cycles are depicted. Cycles drawn using gray and black colors belong to levels 1 and 2, respectively (see Figure 5).

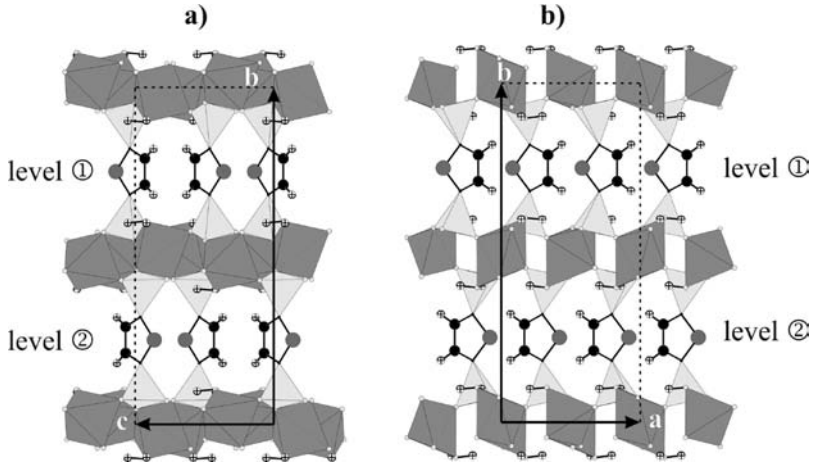

Figure 8. $Mn_2(O_3P{-}C_4H_2S{-}PO_3){\cdot}2H_2O$ **4** projection along the *a* (a) and *b* axes (b).

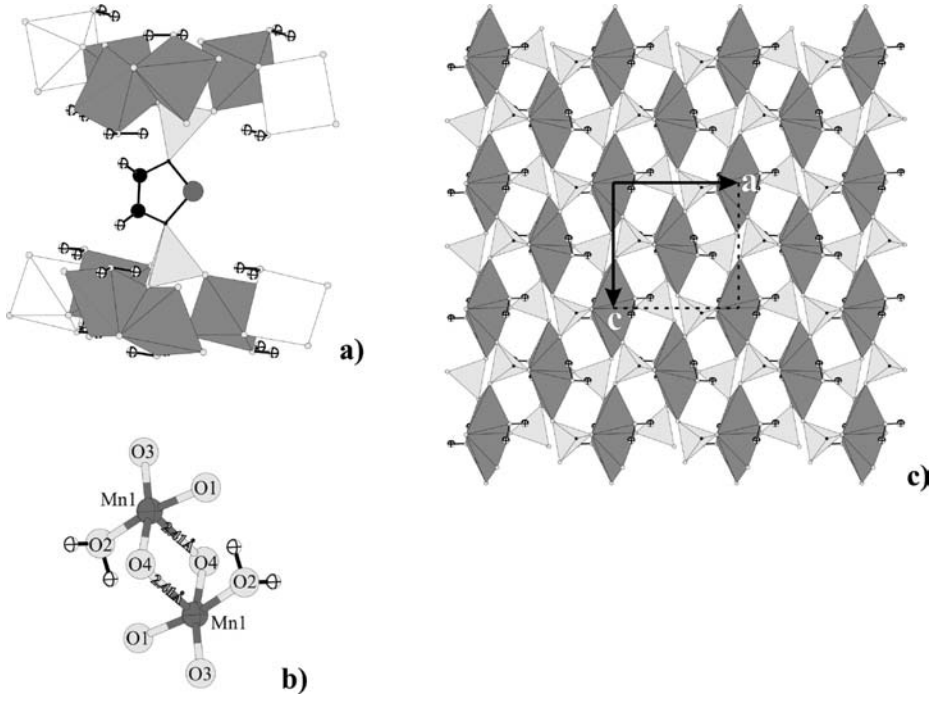

Figure 9. $Mn_2(O_3P{-}C_4H_2S{-}PO_3){\cdot}2H_2O$ **4** (a) view of the connexion between the inorganic layers and the $O_3P{-}C_4H_2S{-}PO_3$ unit (b). Boundary in a $Mn_2O_8H_4$ unit (c) projection along the *c* axis of one inorganic layer (including phosphonate groups).

leads to relatively large interunit Mn−Mn distances (≥4.7 Å) (see Table SI6, Supporting Information). Two consecutive $[Mn_2O_8H_4]_{dimer}$ inorganic planes are connected to the other via the two phosphonic acid functional groups present on the thiophenyl heterocycle in positions 2 and 5 (Figure 9a). Due to the position and the geometry of this spacer ($O_3P{-}C_4H_2S{-}PO_3$) the shortest Mn−Mn interlayer distance ranges from 8.59 to 9.72 Å. In the ($O_3P{-}C_4H_2S{-}PO_3$) organic planes, shown in

dx.doi.org/10.1021/ic301187y | *Inorg. Chem.* 2012, 51, 10251−10261

Figure 8a and 8b, the configuration of these planes is different in levels 1 and 2. The main difference occurs in the orientation of the thiophenyl ring. However, the arrangement of the (C_4H_2S) rings is really revealed in Figure 7b. The (C_4H_2S) cycles form an angle of ~40° with the *a* direction: the rings centered at $z = 1/2$ show a +40° angle, while those centered at $z = 0$ show a −40° angle. Inside the same level (1 or 2 in Figure 8) the (C_4H_2S) cycles are a spaced. The entities of level 1 are shifted of 1/2 *a* in comparison to those of level 2. As a consequence, superposition of the projection along the *b* axis of the two levels exhibits a perfect fishbone arrangement.

The nomenclature proposed by Cheetham and co-workers[38] has been applied to materials **3** and **4** to classify the dimensionality of the inorganic and organic subnetworks. In addition, the inorganic metal oxygen subnetwork corresponds to a 2D dimensionality (I^2), while the organic subnetwork, independent of the orientation of the thiophenyl heterocycle, contributes one order (O^1) to the dimensionality of the resulting material. Consequently, materials **3** and **4** are characterized as having a global dimensionality I^2O^1.

Dehydrated Form $Mn_2(O_3P-C_4H_2S-PO_3)$ **5**. The X-ray powder diffraction experiment performed versus temperature (Figure 4) shows formation above 200 °C of a disordered material corresponding to the dehydrated form of $Mn_2(O_3P-C_4H_2S-PO_3)\cdot 2H_2O$ and called here $Mn_2(O_3P-C_4H_2S-PO_3)$ **5**. Diffraction patterns collected from 200 to 300 °C for $Mn_2(O_3P-C_4H_2S-PO_3)$ present a series of sharp reflections evidencing a loss of crystallinity of the pristine material $Mn_2(O_3P-C_4H_2S-PO_3)\cdot 2H_2O$ **3**. The stacking periodicity of the inorganic layers deduced from the first peak observed on the X-ray powder diffraction (XRPD) pattern in the low-angle region is of 9.3 Å, a value which is in agreement with the stacking distance $d_{002} \approx 9.4$ Å observed for 3. A differential scanning calorimetry (DSC) study, performed on crystallite samples enclosed in an aluminum cap, permitted us to follow the dehydration process. On the basis of thermogravimetric analysis (Figure 10), all scans have been recorded between 10

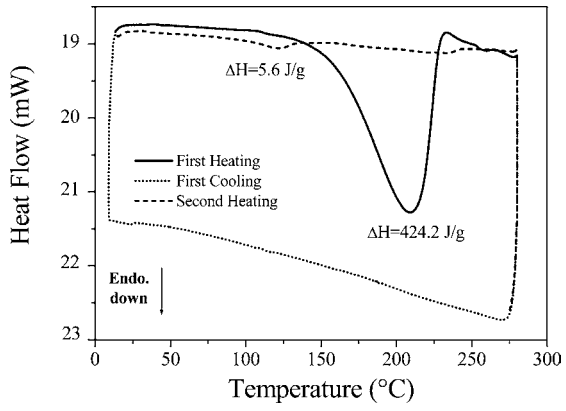

Figure 10. Differential scanning calorimetry curves corresponding to the first heating (line), first cooling (dot), and second heating(dash) of $Mn_2(O_3P-C_4H_2S-PO_3)\cdot 2H_2O$ **3**.

and 280 °C at a rate of 10 °C/min in order to avoid any decomposition of the sample. The first heating scan has from 100 to 230 °C an intense broad endothermic peak which corresponds to dehydration of compound **3** into compound **5**. These temperatures are in good agreement with the temperature of dehydration observed by XRPD as a function of temperature. The enthalpy associated to this phase transformation is 424 J/g (163 kJ/mol). The value of the enthalpy corresponds to those found in the literature for the dehydration process of hydrated coordination compound,[39] and its importance reflects the significant structural changes that occur between the well-crystallized compound **3** and the disordered compound **5**. On the time scale of the DSC experiment, the dehydration process is irreversible since no peak is observed during the first cooling scan. During the second heating scan, the DSC curve has between 100 and 150 °C a small broad endothermic peak with an associated enthalpy of 5.6 J/g. This small value of enthalpy can probably be associated to a transition involving rotation of the thiophene rings from a 'glassy' state to a more disordered state after 100 °C. Of note, the increase of the "flexiblility" of MOF material after dehydration was previously observed by Loiseau et al.[40] Finally, this transition has been observed during all repeating heating and cooling scans recorded by DSC but has never been observed on the PXRD diffractogram recorded during the different heating and cooling cycles. This result indicates that a structural change occurs in the organic network.

Magnetic Properties. The molar magnetic susceptibility χ_{mol} of the hydrated form *hydrated*-$Mn_2(O_3P-C_4H_2S-PO_3)\cdot 2H_2O$ **3** is reported in Figure 11a. A maximum of the magnetic susceptibility χ_{mol} is observed at $T = 19$ K. The magnetic moment is observed to vary linearly with the field at $T = 4$ K up to a field of 5T, with no hysteresis (not shown here). This indicates antiferromagnetic behavior with a Neel temperature $T_N = 19$ K.

The susceptibility for $T > 100$ K can be fitted with a Curie−Weiss law, giving an effective moment $\mu_{eff} = 8.4\ \mu_B$/fu, i.e., 5.94 μ_B per manganese ion, and a Weiss constant $\theta \approx -20$ K (inset of Figure 11b). It is worth noticing that $T_N \approx -\theta$, i.e., the Weiss constant is close to the Neel temperature. This is the result of mean field theory, which implies an unfrustrated magnetic system with long-range interactions. $\mu_{eff} = 5.94\ \mu_B$/Mn is in good agreement with all Mn^{2+} in the high-spin state ($J = S = 5/2$, $\mu_{eff} = 5.92\ \mu_B$). However, for $T < 100$ K, substantial deviation from the Curie−Weiss law is observed, as often reported in low-dimensional magnetic systems. The direction of this deviation is consistent with antiferromagnetic interactions which are more apparent when plotting $\chi_{mol}\cdot T$ versus T (Figure11b). The latter shows a continuous decrease upon cooling. A good fit is obtained using a classical spin Heisenberg model (Fisher model).[41] A value of 6 μ_B per manganese ion and an antiferromagnetic exchange coupling $J/k_B = -44$ K can be inferred from the fitting. Taking into account the different bond lengths between Mn−Mn and Mn−O−Mn described in Table SI3, Supporting Information, the magnetic exchange mechanism is likely a superexchange between two manganese ions through the oxygen ion sharing the corners of the octahedron. The $Mn^{2+}-O-Mn^{2+}$ bond angle is close to 120°. A robust antiferromagnetic interaction is then deduced for the transfert integrals using the Goodenough−Kanamori rules,[42,43] in agreement with our measurements.

The rehydrated $Mn_2(O_3P-C_4H_2S-PO_3)\cdot 2H_2O$ **4** has a layered structure with $Mn_2O_8H_4$ units. The magnetic properties of this phase are notably different from the hydrated phase. As shown in Figure 12a, the antiferromagnetic transition is clearly suppressed. The susceptibility exhibits a Curie−Weiss form with only a weak increase for temperatures less than $T \approx 14$ K. Fitting the data with a Curie−Weiss form gives an effective moment $\mu_{eff} = 8.9\ \mu_B$/fu, i.e., 6.3 μ_B per manganese ion, and a Weiss constant $\theta \approx -67$ K. This latter value shows that

dx.doi.org/10.1021/ic301187y | *Inorg. Chem.* 2012, 51, 10251−10261

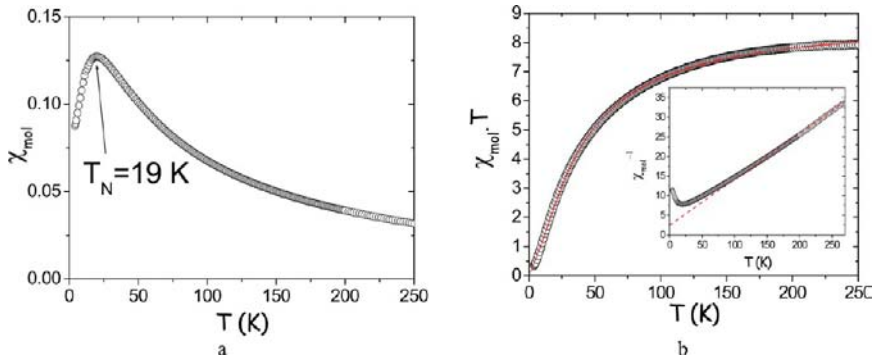

Figure 11. (a) Molar susceptibility of $Mn_2(O_3P{-}C_4H_2S{-}PO_3){\cdot}2H_2O$ **3** with the antiferromagnetic transition at T_N = 19 K. (b) $\chi_{mol}{\cdot}T$ as a function of T. Solid line is the fitting using the Fisher model (classical spin Heisenberg model). (Inset) $1/\chi_{mol}$ as a function of T with the high-temperature Curie–Weiss limit as a dotted line.

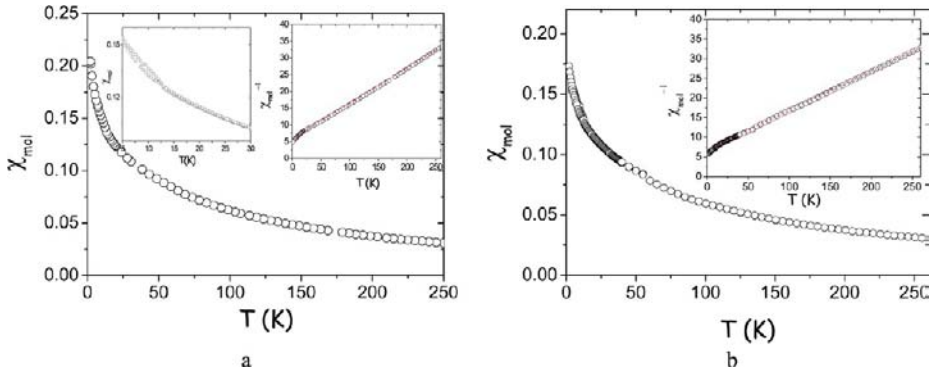

Figure 12. (a) Molar susceptibility of the rehydrated $Mn_2(O_3P{-}C_4H_2S{-}PO_3){\cdot}2H_2O$ **4** as a function of temperature. Note the absence of the antiferromagnetic transition. In the first inset is shown a zoom on the FC-ZFC low-temperature susceptibility. Also shown is $1/\chi_{mol}$ as a function of T . Dotted line is a fit with the high-temperature Curie–Weiss limit. Note the small decrease of susceptibility at low temperature. (b) Molar susceptibility of the dehydrated form $Mn_2(O_3P{-}C_4H_2S{-}PO_3)$ **5**. (Inset) $1/\chi_{mol}$ as a function of T. Dotted line is a fit with the high-temperature Curie–Weiss limit. Note the very small decrease of the inverse of the susceptibility at low temperature.

antiferromagnetic fluctuations are still present, likely via a superexchange mechanism. The value of the magnetic moment is slightly larger than the maximum value of the free Mn^{2+} ion (5.92 μ_B), which has no orbital contribution. This may indicate interacting Mn ions in the dimers. The small increase of the low-temperature susceptibility (more evident when plotting $1/\chi_{mol}$ as a function of T, see the inset of Figure 12a) and the small hysteresis observed in the field-cooling–zero-field-cooling measurements indicate that a very weak ferromagnetism is also present. A weak quantity of ferromagnetic impurities cannot be excluded, but the possibility of an intrinsic mechanism could be addressed. The structure of this sample consists of Mn^{2+} dimers. Compared to the hydrated form, the octahedra are now linked by the edges, the Mn ions are closer, and an examination of the bond lengths indicates that the exchange mechanism can be a direct exchange between the Mn^{2+} ions. In general, there is a critical distance above which ferromagnetic direct exchange is favored.[44] For Mn, the critical distance was found to be 2.8 Å.[45] Here, the main shortest distance between the manganese ions is 3.1 Å, indicating a possible ferromagnetic coupling via direct exchange within dimers in this sample. These dimers are sufficiently isolated to prevent long-range ordering and a genuine ferromagnetic transition.

The magnetic properties of the dehydrated form $Mn_2(O_3P{-}C_4H_2S{-}PO_3)$ **5** are shown in Figure 12b. Its magnetic susceptibility is very close to that of the rehydrated form. In particular, no antiferromagnetic transition is observed, and a Curie–Weiss fit gives similar results: an effective moment μ_{eff} = 6.35 μ_B per manganese ion and a Weiss constant of $\theta \approx -61$ K. A small difference is that the excess of magnetic susceptibility observed at low temperature is lower in $Mn_2(O_3P{-}C_4H_2S{-}PO_3)$ **5**. If intrinsic to the sample, this is consistent with the fact that the structure is strongly disordered, resulting in an averaging of the ferromagnetic component.

CONCLUSION

The hydrated compound $Mn_2(O_3P{-}C_4H_2S{-}PO_3){\cdot}2H_2O$ **3** was synthesized under hydrothermal conditions starting from thiophene-2,5-diphosphonic acid **2**, manganese nitrate, and urea. Its structure was solved by X-ray diffraction on a single crystal and can be described as alternating inorganic layers connected to organic layer via the phosphonate groups. A remarkable feature of the structure of compound **3** is the orientation of the thiophene heterocycles that adopts two different orientations in two successive layers (along c). In one layer the heterocycles are all oriented in the same direction parallel to b, while in the second layer the heterocycles are head-to-tail aligned along a. Dehydration of compound **3** produced the dehydrated material **5** after loss of two water molecules. Of note, this dehydrated material was stable up to 500 °C, pointing out the great stability of the thiophene-2,5-diphosphonic acid moiety. Unfortunately, this material was not crystalline enough for the structure to be solved by X-ray diffraction. Nevertheless, DSC analysis points out a reprodu-

dx.doi.org/10.1021/ic301187y | Inorg. Chem. 2012, 51, 10251–10261

cible low-energy exchange process/transition with an energy exchange around 120 °C that could arise from the reorientation of the thiophene heterocycle. The low crystallinity of this material did not permit validation of this hypothesis by X-ray diffraction. After leaving this dehydrated material **5** at room temperature and ambient humidity for 1 month a polymorph $Mn_2(O_3P-C_4H_2S-PO_3)\cdot 2H_2O$ **4** was isolated, and surprisingly, this material exhibited excellent crystallinity. The main difference between the structures of **3** and **4** arises from both the orientation of the thiophene rings (herringbone-type organization in **4**) and the structure of the inorganic layers. It can be concluded that the thiophene-2,5-diphosphonic acid moieties engaged in materials **3** and **4** adopt different orientations (rotation around the P−C bonds) and the dehydrated state **5**, which is likely more flexible than the hydrated states, allows reorganization of the organic and inorganic network. Finally, the magnetic behavior of compounds **3** and **4** indicates the antiferromagnetic and weak ferromagnetic behavior, respectively, for these two polymorphs. These results are consistent with the structure of these materials. The dehydrated phase **5** presents paramagnetic behavior. This work illustrates the use of thiophene-2,5-diphosphonic acid as a rigid organic building block to design MOF materials and shows the nonreversibility of the dehydration/rehydration process since two polymorphs were characterized. Moreover, this work exemplifies that very soft experimental conditions permitted the rehydration step.

■ ASSOCIATED CONTENT

Supporting Information

Crystallographic data (CIFs; CCDC 424643 and 424642 for **3** and **4**), positional parameters, and hydrogen-bond lengths and angle for compounds **3** and **4**. This material is available free of charge via the Internet at http://pubs.acs.org.

■ AUTHOR INFORMATION

Corresponding Author

*E-mail: jean-michel.rueff@ensicaen.fr (J.-M.R.); pjaffres@univ-brest.fr (P.-A.J.).

Notes

The authors declare no competing financial interest.

■ ACKNOWLEDGMENTS

We thank the "Services Communs" of the University of Brest (RMN-RPE and mass spectrometry) and the technical support of Sylvie Collin of CRISMAT Laboratory for synthesis.

■ REFERENCES

(1) Férey, G. *Dalton Trans.* **2009**, 4400−4415.
(2) Tranchemontagne, D.; Mendoza-Cortés, J. L.; O'Keeffe, M.; Yaghi, O. M. *Chem. Soc. Rev.* **2009**, *38*, 1257−1283.
(3) (a) Bureekaew, S.; Shimomura, S.; Kitagawa, S. *Sci. Technol. Adv. Mater.* **2008**, *9*, 014109. (b) Cheetham, A. K.; Férey, G.; Loiseau, T. *Angew. Chem., Int. Ed.* **1999**, *38*, 3268−3292.
(4) (a) Alsobrook, A. N.; Zhan, W.; Albrecht-Schmitt, T. E. *Inorg. Chem.* **2008**, *47*, 5177−5183. (b) Riou-Cavallec, M.; Sanselme, M.; Guillou, N.; Férey, G. *Inorg. Chem.* **2001**, *40*, 723−725. (c) Serpaggi, F.; Férey, G. *Inorg. Chem.* **1999**, *38*, 4741−4744. (d) Bauer, S.; Bein, T.; Stock, N. *Inorg. Chem.* **2005**, *44*, 5882−5889. (e) Turner, A.; Jaffrès, P. A.; MacLean, E.; Villemin, D.; McKee, V.; Hix, G. B. *Dalton Trans.* **2003**, 1314−1319. (f) Rueff, J. M.; Masciocchi, N.; Rabu, P.; Sironi, A.; Skoulios., A. *Chem.—Eur. J.* **2002**, *8*, 1813−1820.
(5) (a) Devic, T.; David, O.; Valls, M.; Marrot, J.; Couty, F.; Férey, G. *J. Am. Chem. Soc.* **2007**, *129*, 12614−12615. (b) Serre, C.; Stock, N.; Bein, T.; Férey, G. *Inorg. Chem.* **2004**, *43*, 3159−3163. (c) Shi, F. N.; Trindade, T.; Rocha, J.; Paz, F. A. A. *Cryst. Growth Des.* **2008**, *8*, 3917−3920. (d) Rueff, J.-M.; Pillet, S.; Claiser, N.; Bonaventure, G.; Souhassou, M.; Rabu., P. *Eur. J. Inorg. Chem.* **2002**, 895−900.
(6) Bartelet, K.; Marrot, J.; Riou, D.; Férey, G. *Angew. Chem., Int. Ed.* **2002**, *41*, 281−284.
(7) Mao, J. G. *Coord. Chem. Rev.* **2007**, *251*, 1493−1520.
(8) (a) Wu, C. D.; Hu, A.; Zhang, L.; Lin, W. *J. Am. Chem. Soc.* **2005**, *127*, 8940−8941. (b) Seo, J. S.; Whang, D.; Lee, H.; Jun, S. I.; Oh, J.; Young, J.; Kim, K. *Nature* **2000**, *404*, 982−986. (c) Forster, P. M.; Cheetham, A. K. *Top. Catal.* **2003**, *24*, 79−86. (d) Dybtsev, D. N.; Nuzhdin, A. L.; Chun, H.; Bryliakov, K. P.; Talsi, E. P.; Fedin, V. P.; Kim, K. *Angew. Chem., Int. Ed.* **2006**, *45*, 916−920. (e) Sun, C. Y.; Liu, S. X.; Liang, D. D.; Shao, K. Z.; Ren, Y. H.; Su, Z. M. *J. Am. Chem. Soc.* **2009**, *131*, 1883−1888. (f) Cunha-Silva, L.; Lima, S.; Ananias, D.; Silva, P.; Mafra, L.; Carlos, L. D.; Pillinger, M.; Valente, A. A.; Paz, F. A. A.; Rocha, J. *J. Mater. Chem.* **2009**, *19*, 2618−2632.
(9) (a) Rowsell, J. L. C.; Millard, A. R.; Park, K. S.; Yaghi, O. M. *J. Am. Chem. Soc.* **2004**, *126*, 5666−5667. (b) Morris, R. E.; Wheatley, P. A. *Angew. Chem., Int. Ed.* **2008**, *47*, 4966−4981. (c) Latroche, M.; Surble, S.; Serre, C.; Mellot-Draznieks, C.; Llewellyn, P. L.; Chang, J. S.; Jhung, S. H.; Férey, G. *Angew. Chem., Int. Ed.* **2006**, *45*, 8227−8231.
(10) (a) Horcajada, P.; Serre, C.; Maurin, G.; Ramsahye, N. A.; Balas, F.; Vallet-Regi, M.; Seban, M.; Taulelle, F.; Férey, G. *J. Am. Chem. Soc.* **2008**, *130*, 6774−6780. (b) Horcajada, P.; Serre, C.; Vallet-Regi, M.; Sebban, M.; Taulelle, F.; Férey, G. *Angew. Chem., Int. Ed.* **2006**, *45*, 5974−5978. (c) Xiao, B.; Wheatley, P. S.; Zhao, X.; Fletcher, A. J.; Fox, S.; Rossi, A. G.; Megson, I. L.; Bordiga, S.; Regli, L.; Thomas, K. M.; Morris, R. E. *J. Am. Chem. Soc.* **2007**, *129*, 1203−1209. (d) Horcajada, P.; Chalati, T.; Serre, C.; Gillet, B.; Sebrie, C.; Baati, T.; Eubank, J. F.; Heurtaux, D.; Clayette, P.; Kreuz, C.; Chang, J. S.; Hwang, Y. K.; Marsaud, V.; Borie, P. N.; Cynober, L.; Gil, S.; Férey, G.; Couvreur, P.; Gref, R. *Nat. Mater.* **2010**, *9*, 172−178. (e) Josse, S.; Faucheux, C.; Soueidan, A.; Grimandi, G.; Massiot, D.; Alonso, B.; Janvier, P.; Laïob, S.; Pilet, P.; Gauthier, O.; Daculsi, G.; Guicheux, J.; Bujoli, B.; Bouler, J. M. *Biomaterials* **2005**, *26*, 2073−2080. (f) Berchel, M.; Le Gall, T.; Denis, C.; Le Hir, S.; Quentel, F.; Elléouet, C.; Montier, T.; Rueff, J. M.; Salaün, J. Y.; Haelters, J. P.; Lehn, P.; Hix, G. B.; Jaffrès, P. A. *New J. Chem.* **2011**, *35*, 1000−1003.
(11) (a) Lin, X.; Telepeni, I.; Blake, A. J.; Dailly, A.; Brown, C. M.; Simmons, J. M.; Zoppi, M.; Walker, G. S.; Thomas, K. M.; Mays, T. J.; Hubberstey, P.; Champness, N. R.; Schröder, M. *J. Am. Chem. Soc.* **2009**, *131*, 2159−2171. (b) Stylianou, K. C.; Heck, R.; Chong, S. Y.; Bacsa, J.; Jones, J. T. A.; Khimyak, Y. Z.; Bradshaw, D.; Rosseinsky, M. J. *J. Am. Chem. Soc.* **2010**, *132*, 4119−4130. (c) Doonan, C. J.; Morris, W.; Furukawa, H.; Yaghi, O. M. *J. Am. Chem. Soc.* **2009**, *131*, 9492−9493.
(12) (a) Clearfield, A. *Prof. Inorg. Chem.* **1998**, *47*, 371−510. (b) Clearfield, A. *Curr. Opin; Solid State Mater. Sci.* **2003**, *6*, 495−506. (c) Clearfield, A. *J. Alloys Comp.* **2006**, *418*, 128−138. (d) Le Bideau, J.; Bujoli, B.; Jouanneaux, A.; Payen, C.; Palvadeau, P.; Rouxel, J. *Inorg. Chem.* **1993**, *32*, 4617−4620.
(13) Song, J. J.; Lei, C.; Sun, Y. Q.; Mao, J. G. *J. Solid State Chem.* **2004**, *177*, 2557−2564.
(14) (a) Xiao, B.; Byrne, P. J.; Wheatley, P. S.; Wragg, D. S.; Zhao, X.; Flechter, A. J.; Thomas, K. M.; Peters, L.; Evans, J. S. O.; Warren, J. E.; Zhou, W.; Morris, R. E. *Nat. Chem.* **2009**, *1*, 289−294. (b) Allan, P. K.; Xiao, B.; Teat, S. J.; Knight, J. W.; Morris, R. E. *J. Am. Chem. Soc.* **2010**, *132*, 3605−3611.
(15) Hix, G. B.; Caignaert, V.; Rueff, J. M.; Le Pluart, L.; Warren, J. E.; Jaffrès, P. A. *Cryst. Growth Des.* **2007**, *7*, 208−211.
(16) (a) Hix, G. B.; Turner, A.; Kariuki, B. M.; Tremayne, M.; MacLean, E. J. *J. Mater. Chem.* **2002**, *12*, 3220−3227. (b) Maeda, K. *Microporous, Mesoporous Mater.* **2004**, *73*, 47−55.
(17) Rueff, J. M.; Perez, O.; LeClaire, A.; Couthon-Gourvès, H.; Jaffrès, P. A. *Eur. J. Inorg. Chem.* **2009**, 4870−4876.
(18) Rueff, J. M.; Barrier, N.; Boudin, S.; Dorcet, V.; Caignaert, V; Boullay, P.; Hix, G. B.; Jaffrès, P. A. *Dalton Trans.* **2009**, 10614−10620.

(19) Rueff, J. M.; Caignaert, V.; Leclaire, A.; Simon, C.; Haelters, J. P.; Jaffrès, P. A. *CrystEngComm* **2009**, *11*, 556−559.
(20) Rueff, J. M.; Caignaert, V.; Chausson, S.; Leclaire, A.; Simon, C.; Perez, O.; Le Pluart, L.; Jaffrès, P. A. *Eur. J. Inorg. Chem.* **2008**, 4117−4125.
(21) Rueff, J. M.; Perez, O.; Simon, C; Couthon-Gourvès, H.; Lorilleux, C.; Jaffrès, P. A. *Cryst. Growth Des.* **2009**, *9*, 4262−4268.
(22) (a) Huang, W.; Wu, D.; Zhou, P.; Yan, W.; Guo, D.; Duan, C.; Meng, Q. *Cryst. Growth Des.* **2009**, *9*, 1361−1369. (b) Gong, Y.; Wang, T.; Zhang, M.; Hu, C. W. *J. Mol. Struct.* **2007**, *833*, 1−7. (c) Eddaoudi, M.; Kim, J.; Vodak, D.; Sudik, A.; Wachter, J.; O'Keeffe, M.; Yaghi, O. M. *Proc. Natl. Acad. Sci. U.S.A.* **2002**, *99*, 4900−4904. (d) Chen, B. L.; Mok, K. F.; Ng, S. C.; Drew, M. G. B. *New J. Chem.* **1999**, *23*, 877−883.
(23) (a) Wang, J. G.; Huang, C. C.; Huang, X. H.; Liu, D. S. *Cryst. Growth Des.* **2008**, *8*, 795−798. (b) Chen, Z.; Zuo, Y.; Li, X. H.; Wang, H.; Zhao, B.; Shi, W.; Cheng, P. *J. Mol. Struct.* **2008**, *888*, 360−365.
(24) Zhang, J.; Chen, S.; Wu, T.; Feng, P.; Bu, X. *J. Am. Chem. Soc.* **2008**, *130*, 12882−12883.
(25) Demessence, A.; Rogez, G.; Rabu, P. *Chem. Mater.* **2006**, *18*, 3005−3015.
(26) Gerbier, P.; Guérin, C.; Henner, B.; Unal, J. R. *J. Mater. Chem.* **1999**, *9*, 2559−2565.
(27) Hsu, C. W.; Wang, L.; Su, W. F. *J. Colloid Interface Sci.* **2009**, *329*, 182−187.
(28) (a) Tavs, P. *Chem. Ber.* **1970**, *103*, 2428−2436. (b) Krasil'nikova, E. A.; Nevzorova, O. L.; Sentenov, V. V. *Zh. Obsch. Khim.* **1985**, *55*, 1283−1287.
(29) Demessence, G.; Rogez, R.; Walter; Rabu, P. *Inorg. Chem.* **2007**, *46*, 3423−3425.
(30) Duisenberg, J.; Kroon-Batenburg, M.; Schreurs, M. *J. Appl. Crystallogr.* **2003**, *36*, 220−229.
(31) Sheldrick, G. M. *SADABS*; Bruker AXS Inc.: Madison, WI, 2002.
(32) Oszlanyi, G.; Suto, A. *Acta Crystallogr.* **2004**, *A60*, 134−141.
(33) Palatinus, L.; Chapuis, G. *J. Appl. Crystallogr.* **2007**, *40*, 786−790.
(34) Palatinus, L.; van der Lee, A. *J. Appl. Crystallogr.* **2008**, *41*, 975−984.
(35) Petricek, V.; Dusek, M.; Palatinus, L. *JANA2006, The crystallographic computing system*; Institute of Physics: Praha, Czech Republic, 2006.
(36) Brown, I. D. *J. Appl. Crystallogr.* **1996**, *29*, 479−480.
(37) Flack, H. D. *Acta Crystallogr.* **1983**, *A39*, 876−881.
(38) Cheetham, A. K.; Rao, C. N. R.; Feller, R. K. *Chem. Commun.* **2006**, *46*, 4780−4795.
(39) Berbenni, V.; Marini, A.; Bruni, G.; Riccardi, R. *Thermochim. Acta* **2000**, *346*, 115−132.
(40) Volkringer, C.; Loiseau, T.; Guillou, N.; Férey, G.; Haouas, M.; Taulelle, F.; Audebrand, N.; Margiolaki, I.; Popov, D.; Burghammer, M.; Riekel, C. *Cryst. Growth Des.* **2009**, *9*, 2927−2936.
(41) Fisher, M. E. *Am. J. Phys.* **1964**, *32*, 343−346.
(42) Goodenough, J. B. *J. Phys. Chem. Solids* **1988**, *6*, 287−297.
(43) Kanamori, J. *J. Phys. Chem. Solids* **1959**, *10*, 87−98.
(44) Slater, J. C. *Phys. Rev.* **1930**, *36*, 57−64.
(45) Forrer, R. *Ann. Phys.* **1952**, *7*, 605−621.